Eur Radiol (2011) 21:841–849
DOI 10.1007/s00330-010-1962-9

MAGNETIC RESONANCE

Renal imaging at 7 Tesla: preliminary results

Lale Umutlu · Stephan Orzada · Sonja Kinner · Stefan Maderwald · Irina Brote · Andreas K. Bitz · Oliver Kraff · Susanne C. Ladd · Gerald Antoch · Mark E. Ladd · Harald H. Quick · Thomas C. Lauenstein

Received: 28 April 2010 / Revised: 2 August 2010 / Accepted: 3 August 2010 / Published online: 25 September 2010

Abstract
Objective To investigate the feasibility of 7T MR imaging of the kidneys utilising a custom-built 8-channel transmit/receive radiofrequency body coil.
Methods In vivo unenhanced MR was performed in 8 healthy volunteers on a 7T whole-body MR system. After B_0 shimming the following sequences were obtained: 1) 2D and 3D spoiled gradient-echo sequences (FLASH, VIBE), 2) T1-weighted 2D in and opposed phase 3) True-FISP imaging and 4) a T2-weighted turbo spin echo (TSE) sequence. Visual evaluation of the overall image quality was performed by two radiologists.
Results Renal MRI at 7T was feasible in all eight subjects. Best image quality was found using T1-weighted gradient echo MRI, providing high anatomical details and excellent conspicuity of the non-enhanced vasculature. With successful shimming, B_1 signal voids could be effectively reduced and/or shifted out of the region of interest in most sequence types. However, T2-weighted TSE imaging remained challenging and strongly impaired because of signal heterogeneities in three volunteers.
Conclusion The results demonstrate the feasibility and diagnostic potential of dedicated 7T renal imaging. Further optimisation of imaging sequences and dedicated RF coil concepts are expected to improve the acquisition quality and ultimately provide high clinical diagnostic value.

Keywords High-field MRI · 7 Tesla MRI · Kidney MRI · Renal imaging · Ultra highfield imaging

L. Umutlu (✉) · S. Orzada · S. Kinner · S. Maderwald · I. Brote · A. K. Bitz · O. Kraff · S. C. Ladd · G. Antoch · M. E. Ladd · H. H. Quick · T. C. Lauenstein
Department of Diagnostic and Interventional Radiology and Neuroradiology, University Hospital Essen,
Hufelandstr. 55,
Essen, Germany
e-mail: Lale.Umutlu@uk-essen.de

L. Umutlu · S. Orzada · S. Kinner · S. Maderwald · I. Brote · A. K. Bitz · O. Kraff · S. C. Ladd · G. Antoch · M. E. Ladd · H. H. Quick · T. C. Lauenstein
Erwin L. Hahn Institute for Magnetic Resonance Imaging,
Essen, Germany

Introduction

Magnetic resonance imaging of the kidneys has gained an important role in clinical routine. MRI is coupled with higher sensitivity and specificity rates regarding the depiction of most neoplastic diseases of abdominal solid organs compared with ultrasound or computed tomography (CT) [1]. Utilisation of MRI at 1.5T is considered the clinical standard in most centres. However, high-field MRI of the abdomen at 3T has been proven to be feasible over the last few years [2–9]. An increase in the magnetic field strength is associated with increased signal-to-noise ratio (SNR). The resulting improved contrast-to-noise ratio (CNR) has been shown to be beneficial in various applications of diagnostic high-field MRI [2, 3]. Several studies have demonstrated the successful transformation of the associated higher SNR into a higher spatiotemporal resolution, enabling an improvement in the assessment of anatomical details as well as increased accuracy for the depiction of pathological findings [9–13]. In a first clinical study in patients with Multiple Sclerosis, Kollia et al. demonstrated the diagnostic superiority of 7 Tesla MRI for the detection and delineation of MS lesions. In comparison to 1.5 Tesla MRI, ultra-high-field MR imaging provided improved visualisation of the MS lesions in the white and grey

matter and superiorly presented structural abnormalities within the lesions [10]. Maderwald et al. published a study demonstrating the high diagnostic value of non-enhanced T1 weighted imaging for intracranial MRA at 7 Tesla [11]. These promising results of high quality ultra-high-field imaging of parenchyma and vessels of the neurocranium, form the theoretical basis for investigations in the abdomen.

However, other physical effects associated with higher magnetic field strengths may impair diagnostic imaging. An increase in the magnetic field strength can provoke artefacts because of changes in tissue susceptibility, chemical shift, or signal heterogeneities due to radiofrequency (RF) wavelength effects [8, 14, 15]. Furthermore, the energy deposited by RF waves is known to be restrictive at high-field imaging, as the RF absorption increases proportionally to the square of the static magnetic field. Despite these outlined limitations, 3T renal MRI has been nearing readiness for implementation into clinical standards.

Ultra-high-field MR imaging at 7T has recently become available for in vivo human imaging. Most trials evaluating ultra-high-field MRI have focused on neurological and musculoskeletal imaging [10–13, 16, 17]. First approaches to 7T whole-body MRI, published by Vaughan et al., have demonstrated the potential of this technique, but also the need for further investigation with regard to RF technology and sequence optimisation [18].

The aim of this study was to investigate the feasibility of dedicated 7T MR imaging of the kidneys utilising a custom-built 8-channel transmit/receive RF body coil on a 7 Tesla whole-body MR system.

Materials and methods

Study population

In vivo 7T measurements were performed in eight healthy volunteers (four male and four female; average age: 29.3 years, range 26–33 years). The study was conducted in accordance with all guidelines set forth by the approving institutional review board. Written informed consent was obtained before each examination.

MR and coil system

Examinations were performed in the supine position on a 7T whole-body MR system (Magnetom 7T, Siemens Healthcare Sector, Erlangen, Germany). The system was equipped with a gradient system enabling 45 mT/m maximum amplitude and a slew rate of 220 mT/m/ms.

For image acquisition, a custom-built body transmit/receive RF coil was used, consisting of symmetrically excited meander elements, providing higher intrinsic decoupling in coil arrays and larger penetration depth in the imaged subject than common strip line elements. The body coil is composed of two arrays with 4 elements each placed ventrally and dorsally on the upper half of the abdomen (Fig. 1). The elements of the ventral array are enclosed in individual modules made of Macrolon, interconnected with a Neoprene sheet to provide the flexibility to adapt to the shape of the individual patient's anatomy and ensure best possible B_1^+ uniformity. The elements of the dorsal array are arranged in a plane on a sliding frame, which can be moved back and forth to position the array relative to the patient along the longitudinal axis [19].

In comparison to 1.5T imaging, high-field MRI is known to be restrained by B_1 field heterogeneities because of the reduced Larmor wavelength at 7T of approximately 12 cm, leading to destructive B_1 interference (signal voids) within the acquired FOV. Hence, an add-on system for RF shimming was integrated on the small signal side of the MR system to mitigate the above-mentioned heterogeneities [20]. The RF amplifier of the unmodified MR system consists of eight individual modules providing 1 kW each (LPPA 12080W, Dressler, Germany), that are combined to provide 8 kW of RF power in the single-channel configuration. After hardware and software modification, RF shimming could be implemented by splitting the excitation signal of the conventional single-channel system into 8 independent channels. The system-enabled application of optimised sets of

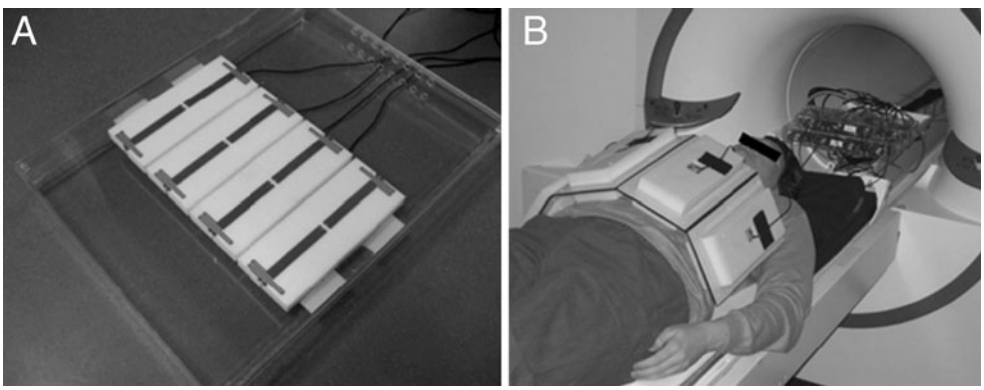

Fig. 1 Dorsal 4-channel transmit/receive RF array with four stripline meander elements (**a**) and flexible ventral 4-channeltransmit/receive RF array, also composed of four stripline meander elements, positioned on top of a volunteer (**b**)

amplitude and phase shifts to achieve a uniform excitation of specific body regions. Real-time RF supervision was performed by use of logarithmic power meters monitoring forward and reflected power of all eight channels. A real-time field programmable gate array (NI PXI 7852R, National Instruments, Austin, TX, USA) provided time-averaging of the transmitted RF power according to IEC safety guidelines [20].

Specific Absorption Rate (SAR) calculations were performed in a male human body model (HUGO) derived from the Visible Human Project using FDTD simulations (CST Microwave Studio, CST AG, Darmstadt, Germany), as well as in the adult male (Duke) and adult female (Ella) models of the Virtual Family [21].

Examination protocol and sequence modification

Subsequent to B_0 shimming using a vendor-provided gradient echo sequence and algorithm, B_1 shimming was performed with the custom 8-channel B_1 shimming system in the region-of-interest (ROI), i.e. the kidneys. By using a phase increment of 90° between neighbouring coil elements and equal amplitudes (second-order birdcage mode, CP^{2+} mode) for axial imaging, a focal periaortal signal void was produced, enabling a better delineation of the ROI. For coronal imaging a phase increment of 45° between neighbouring elements and equal amplitudes (first-order birdcage mode, CP mode) was used, transitioning the signal voids out of the ROI to the right upper quadrant of the abdomen.

The following sequences were acquired.

1. Coronal T1-weighted 3D spoiled gradient-echo sequence (3D FLASH).
2. Coronal T1-weighted 2D spoiled gradient-echo sequence (2D FLASH).
3. Axial T1-weighted 2D in and opposed phase gradient-echo sequence.
4. Coronal T2-weighted true fast imaging with steady-state precession (TrueFISP).
5. Axial T2-weighted turbo spin echo (TSE) sequence.

Imaging parameters [repetition time (TR), echo time (TE), flip angle (α), and bandwidth] had to be adapted and modified to 7 Tesla while maintaining subjectively comparable contrast results with regard to standard 1.5 Tesla sequences.

T1-weighted 2D FLASH imaging was modified to provide high-definition anatomy at high spatial resolution with a 1024×1024 interpolated acquisition matrix, resulting in a considerably reduced temporal resolution with the need for 3 measurements (13 slices each) for full organ coverage. Subjectively optimal T1 contrast was found to be achieved with a TR of 130 ms and TE of 3.57 ms. High quality and homogeneous fat saturation of the subcutaneous and intra-abdominal fat was obtained, resulting in excellent inter-organ differentiation.

As dynamic imaging demands repeated consecutive measurements, sequence parameters of the 3D FLASH sequence were selected to remain within a breath-hold acquisition time of 24 s and provide full organ coverage. Hence, the highest achievable spatial resolution under these constraints was determined to be an interpolated acquisition matrix of 640×640 (0.63 mm² in-plane resolution) with a slice thickness of 1.6 mm. As in all other coronal imaging sequences, FOV for 3D FLASH imaging was maintained at 400×400 mm².

In-phase and opposed phase gradient echo imaging was obtained in axial orientation with an interpolated acquisition matrix of 640×480 with a FOV of 340×255 mm^2. In-phase imaging was acquired with a TR/TE of 140 ms/2.04 ms and opposed phase imaging with a TR/TE of 140 ms/3.57 ms.

For T2w TSE imaging a multi-slice breath-hold TSE sequence was applied. Despite utilisation of a reduced nominal refocusing flip angle of 120°, SAR limitations remained a major constraint for the TSE sequence, limiting the maximum number of slices per acquisition to 16 slices; a thickness of 5.5 mm thus provided full kidney coverage within a breath-hold. To mitigate energy deposition, parallel imaging and variable refocusing flip angles were applied; however, TSE imaging remained highly challenging and strongly impaired.

The detailed sequence parameters are summarised in Table 1. The total in-room time for each examination was assessed using a stop watch. After leaving the MRI room, all subjects were asked about the side effects and their acceptance of the examination time, positioning, and sensations such as vertigo or nausea.

Image analysis and statistical evaluation

All MR images were analysed on a standard Picture Archiving and Communication System (PACS) workstation (Centricity RIS 4.0i, GE Healthcare, USA). Visual evaluation of the image quality for each sequence type was performed by two radiologists with 11 and 8 years' experience in abdominal MRI using a three-point scale (1 = poor, 2 = moderate, 3 = good quality). The evaluation was based on (1) the cortico-medullary differentiation and the delineation of (2) adrenal glands, (3) proximal ureter, (4) renal arteries, and (5) renal veins. The presence of artefacts was assessed using a three-point scale (1 = strong impairment 2 = slight impairment of image quality, 3 = no artefact present or insignificant). For statistical analysis, Wilcoxon's Rank Test was used. Score values of image quality and presence of artefacts for each sequence were compared. For the adaptation to multiple samples, a Bonferroni correction was used. A p value$<$ 0.05 was considered to establish statistically significant differences.

Table 1 Imaging parameters for the 7T kidney protocol

	2D FLASH	3D FLASH	In and Opp. Phase GRE	TrueFISP	T2w TSE
Slice orientation	coronal	coronal	axial	coronal	axial
Fat saturation	yes	yes	none	none	yes
Repetition time TR [ms]	130	2.9	140	3.48	3060
Echo time TE [ms]	3.57	1.02	2.04 / 3.57	1.53	99
Nominal Flip angle FA [°]	70	10	65	50	120
Bandwidth [Hz/pixel]	410	920	920 / 980	977	130
Field-of-view FOV [mm²]	400×400	400×400	340×255	400×400	350×240
Acquisition matrix [pixel]	512×512	320×320	320×240	320×256	256×176
Interpolated to	1024×1024	640×640	640×480	640×512	512×382
Voxel volume [mm³] non-interpolated	0.8×0.8×2.0	1.3×1.3×1.6	1.1×1.1×3.0	1.3×1.6×4.0	1.4×1.4×5.5
Slice thickness [mm]	2	1.6	3	4	5.5
Slices	13	128	10	21	16
Parallel acquisition with GRAPPA (reference lines)	2 (24)	2 (24)	2 (48)	none	2 (43)
Acquisition time [sec]	31	27	20	19	34

Results

All 7T examinations were performed successfully and were well tolerated by the subjects without any side effects. The mean examination time amounted to 25 min (+/- 7 min), including patient positioning, shimming and data acquisition. Best overall image quality was found for the 2D FLASH sequence with an average score of 2.45. This value was significantly higher compared with the 3D FLASH, TrueFISP, and theT2-weighted sequence with p values<0.0005. The 2D FLASH sequence also proved to be least prone to artefacts (mean score: 2.64) and showed statistically significantly less impairment by artefacts than the T2-weighted sequence (mean score: 1.43). All results for image quality and presence of artefacts are displayed in Tables 2 and 3. Detailed results for each sequence are listed below.

2D T1-weighted spoiled gradient-echo sequence (2D FLASH)

Qualitative image analysis revealed high scores for the 2D FLASH images in the demarcation of corticomedullary differentiation (mean score: 2.64), as well as the proximal ureter (2.21) and adrenal glands (1.86) (Fig. 2a). Despite the lack of intravenous contrast medium administration, renal vasculature showed high signal intensity and was well delineated (mean renal arteries 2.9; mean renal veins 2.64). In particular the arterial vasculature was well depicted from the renal hilum to the peripheral cortex (Fig. 2b, c). Because of shimming, the region of interest was well assessable in all subjects, as minor B_1 heterogeneities could be shifted to the circumjacent abdomen (mean impairment value: 2.64).

3D T1-weighted spoiled gradient-echo sequence (3D FLASH)

Owing to the high spatial resolution, the kidneys were well visualised and good corticomedullary differentiation could be achieved (mean score: 2.07; Fig. 3). However the low perirenal fat saturation impeded a good delineation of the adrenal glands (1.0) and the proximal ureter (mean score: 1.64). The high signal intensity of the arterial vasculature provided excellent visualisation (mean score: 2.71; Fig. 4a). Thus, the anatomical variant of an accessory left renal artery was found in one volunteer (Fig. 4b). Only a moderate mean score (1.86)

Table 2 Mean values of qualitative image evaluation (1 = poor, 2 = moderate, 3 = good quality)

Anatomical structure	2D FLASH	3D FLASH	In and Opposed Phase GRE	TrueFISP	T2w TSE
Corticomedullary differentiation	2.64	2.07	2.36	1.43	1.64
Adrenal glands	1.86	1.00	2.43	1.00	1.50
Ureter	2.21	1.64	1.43	1.79	1.64
Renal arteries	2.90	2.71	2.43	1.71	1.10
Renal veins	2.64	1.86	1.64	1.36	1.00
Overall image quality	**2.45**	**1.86**	**2.06**	**1.46**	**1.38**

Table 3 Mean values of qualitative evaluation of image impairment due to artefacts (1 = strong impairment, 2 = slight impairment of image quality, 3 = no artefact present or insignificant)

2D FLASH	3D FLASH	In and Opposed Phase GRE	TrueFISP	T2w TSE	Overall image impairment
2.64	2.36	2.21	1.93	1.43	**2.11**

was found for the depiction of the venous vasculature, as only low signal intensity of the renal veins was observed. Imaging was moderately impaired by RF field heterogeneities with an overall image impairment score of 2.36.

T1-weighted 2D in and opposed phase GRE sequence

The mean image quality score for in and opposed phase T1w-imaging amounted to 2.06, with highest values for the corticomedullary differentiation and the depiction of the adrenal glands and renal arteries (each 2.4 on average). Lowest image quality was found for the depiction of the ureter (1.43). Opposed phased imaging revealed the typical sharply defined black rim around organs with a fat/water interface (Fig. 5). Mean artefact score amounted to 2.21. In 2 out of the 8 subjects, B_1 heterogeneities could not be mitigated effectively, leaving the evaluation of the right kidney impeded.

T2-weighted true fast imaging with steady-state precession (TrueFISP)

TrueFISP imaging provided only moderate image quality, with an overall mean score of 1.46 and ranging between 1.00 (adrenal glands) and 1.79 (visualisation of the ureter). Banding artefacts were present in the region of interest in 4 out of the 8 subjects, decreasing the overall image quality (mean artefact score: 1.93) (Fig. 6a). In addition, chemical shift artefacts at the margins of the kidney could be depicted (Fig. 6b).

T2-weighted TSE sequence

T2-weighted TSE imaging remained challenging because of B_1 field heterogeneities and TSE's SAR-intensive nature. Diagnostic values were limited in 3 out of the 8 subjects (Fig. 7a). TSE imaging showed the strongest impairment of all evaluated sequences, with a mean value of 1.43 and an average image quality index of 1.38. While the visualisation of the corticomedullary differentiation and the ureter was best (mean score: 1.64), visualisation of the renal veins was associated with the lowest mean score of 1.00.

Discussion

The current study carries three messages we believe to be important. First, dedicated in vivo MRI of the kidneys is feasible at 7T providing there is good overall image quality

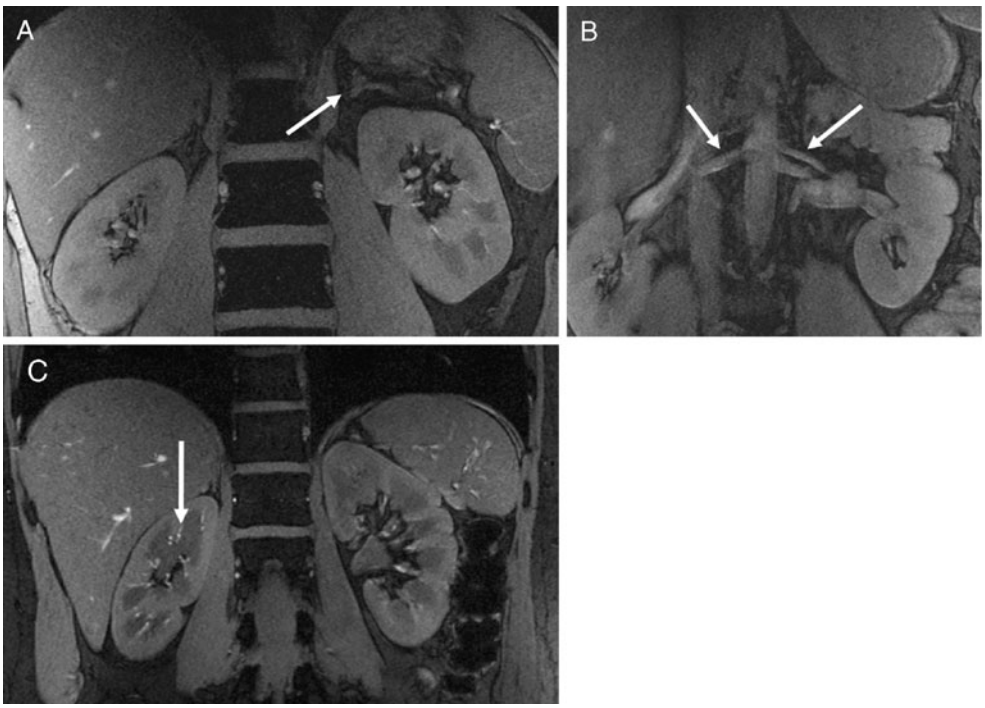

Fig. 2 2D FLASH images: Effective fat saturation enabled very good inter-organ differentiation and depiction of small anatomical structures such as the adrenal glands (arrow **a**). Because of the inherently high signal intensity of the vasculature, 2D FLASH imaging reveals an excellent depiction of the renal vasculature (arrow **b**), including small renal arteries at the transition of the medulla to the cortex (**c**)

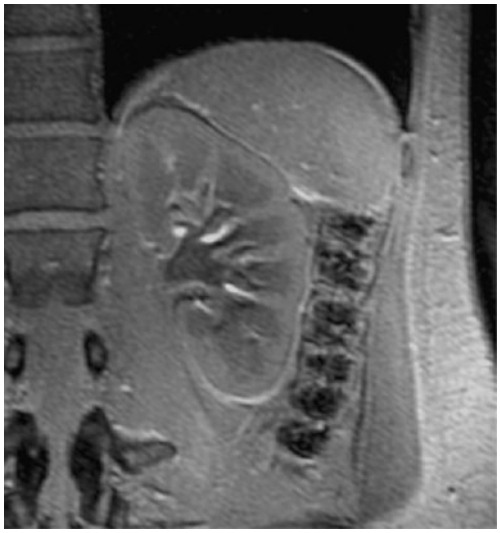

Fig. 3 3D FLASH imaging revealed very good corticomedullary differentiation as shown here for the left kidney

of the region of interest. Second, T1w GRE imaging showed excellent results regarding the differentiation of small anatomical structures and even allowed for a robust assessment of the renal vasculature without intravenous contrast medium administration. Possibly, T2w TSE and TrueFISP imaging are currently limited at 7T due to artefacts and SAR restrictions.

Ultra-high-field MRI at 7T has only recently become available for in vivo applications in humans and has yet to achieve its full potential due to multiple technical challenges. First implementations have been based on neurological and musculoskeletal imaging, as only circumscribed anatomical structures with limited cross-section are visualised and restrictions due to motion artefacts can be avoided. In these anatomical areas, 7T MRI has verified its diagnostic potential [10–13, 16, 17]. Owing to advances in RF coil concepts and the ability to perform transmit RF field (B_1) shimming, in vivo applications of high-field MRI have recently been expanded to cardiac and even whole-body imaging [18, 22]. Vaughan et al. recently published the preliminary results of whole-body MRI at 7 Tesla using a custom-built detunable transverse electromagnetic body coil and a 16-channel transmit/receive surface coil. Coronal, sagittal and transaxial multislice image sets were acquired [18]. It could be shown that whole-body MRI at 7T using body coils was impaired because of heterogeneous excitation. However, utilisation of the 16-channel RF surface coil resulted in better image quality in dedicated anatomical areas including the heart. The same group presented in a subsequent trial the first results of cardiac imaging at 7 Tesla [22]. Anatomical and functional images could be acquired using an eight-channel surface coil in conjunction withB_1 shimming. The preliminary results of both studies demonstrate the potential of ultra-high-field imaging in the thorax and abdomen, but also underline the need for further development of RF technology and sequence adjustment. First successful imaging results in cardiac and abdominal imaging utilising a custom-built 8-channel transmit/receive array with an8-channel add-on RF shimming system have also recently been demonstrated by Bitz et al. and Maderwald et al., showing the potential for uniform excitation of specific body regions [19, 20, 23].

To our knowledge the current trial is the first study specifically demonstrating the feasibility of MRI of the kidneys at 7T. Similar to the study by Vaughan et al. and Snyder at al. [18, 22], a multi-channel array coil was utilised and B_1 shimming was performed to improve data acquisition. This is crucial, as ultra-high-field imaging is known to be susceptible to RF heterogeneities because of the short RF wavelength at 300 MHz, leading to major signal intensity variations across the image. With the implementation of a static add-on RF shimming system, a homogeneous signal could be achieved in the region-of-interest. Additionally, on-line RF supervision was provided throughout image acquisition to ensure the examined subjects' safety.

However, there were considerable differences between T1w- and T2w imaging with regard to image quality, conspicuity of anatomical details, and presence of artefacts. T1w GRE images provided excellent corticomedullary differentiation. This may be particularly helpful for the specification of renal tumours, as renal cell carcinomas (RCC) arise from the proximal renal tubular epithelium while renal transitional cell carcinoma (TCC) originates

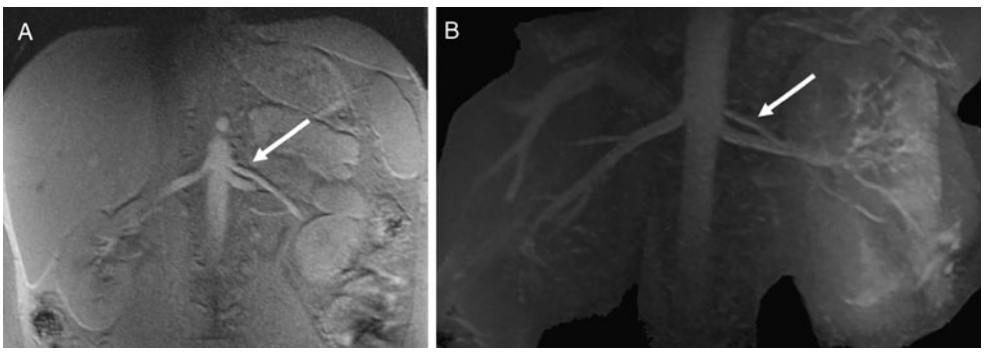

Fig. 4 3D FLASH imaging provided excellent conspicuity of the arterial vasculature (**a**). Owing to the inherently high vascular signal, a Maximum-Intensity-Projection (MIP) in coronal orientation (**b**) provides good visualisation of the abdomnal aorta and the renal arteries. Arrows point at an incidentally diagnosed left accessory renal artery

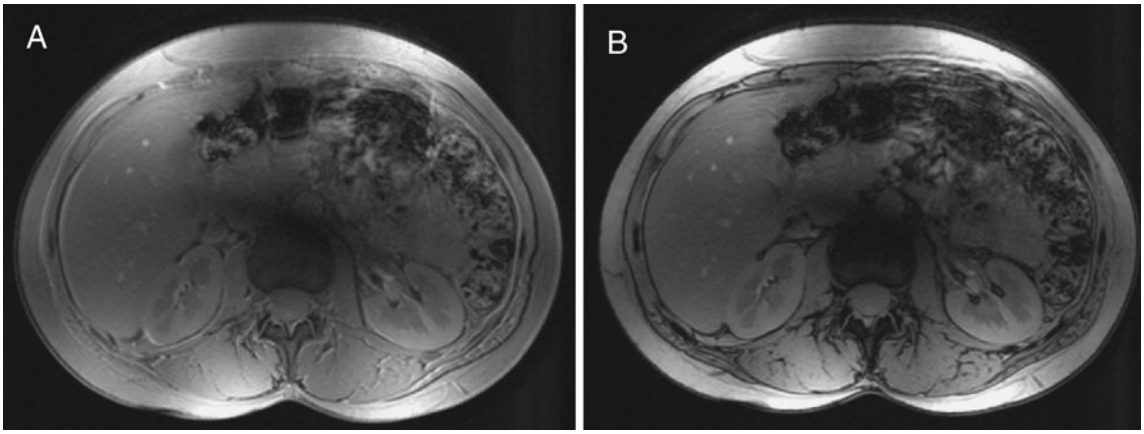

Fig. 5 In-plane and opposed phase imaging (**a** and **b**). Via successful shimming (using the CP^{2+} mode of the coil), impeding B_1 heterogeneities could be shifted ventral to the region of interest. Opposed phase images provide typical sharply defined black rims around organs with a fat/water interface (**b**)

from the urothelium in the medulla [24]. Furthermore, T1w imaging with fast gradient echo-based sequences allowed for a robust depiction of the renal vessels without the need for intravenous gadolinium administration. The inherently hyperintense vessel-to background contrast at 7T has been observed in other anatomical regions [11, 22]. The aetiology of the high vascular T1 signal at 7T remains incompletely evaluated at this point, but inflow and steady-state effects may be accountable. Furthermore, unlike conventional 1.5T and 3T MR systems using a large volume built-in transmit body RF coil, 7 Tesla MRI at this point uses local transmit/receive RF coils. In this case, the flowing spins are not pre-saturated by RF pulses when they enter the imaging region. Thus, inflowing spins can be considered "fresh" and contribute to the hyperintense blood signal.

This fact may have some impact on clinical applications, too. Intravenous administration of certain gadolinium compounds has been shown to be associated with nephrogenic systemic fibrosis (NSF) in patients with impaired renal function [25]. Hence, ultra-high-field MR angiography might provide information on the renal vasculature with a high spatial resolution, but without the need for intravenous gadolinium. On the other hand, the benefit of intravenous gadolinium administration for renal MRI at 7T has not yet been evaluated. Contrast medium administration will be the focus of ongoing studies if dynamic T1w imaging and perfusion analysis of renal tissue can be successfully implemented.

We were also able to demonstrate the feasibility of in- and opposed phase T1w imaging with good visualisation of the adrenal glands as well as the kidneys. Again, it is conceivable that this technique will have a strong impact on future 7T MRI applications in a clinical setting. In particular the classification of fatty tissue due to signal loss at water/fat interfaces on opposed-phase imaging is crucial in delineating and specifying adrenal and renal tumours.

TrueFISP imaging offered a moderate anatomical overview of abdominal structures by providing a mixture of both T1 and T2 contrast. However, due to its sensitive nature regarding B_0 heterogeneity, imaging remained impaired by banding artefacts at air/tissue interfaces.

Clearly, the present trial is not without some significant limitations. The image quality of T2w MRI was strongly impaired in 3 out of 8 volunteers. This is mainly due to the residual B_1 field heterogeneities at ultra-high magnetic field strength even after B_1 shimming, as they impede the generation of accurate refocusing pulses, which form the basis of good quality TSE imaging. Also, due to RF amplifier restrictions, maximum flip angles were limited.

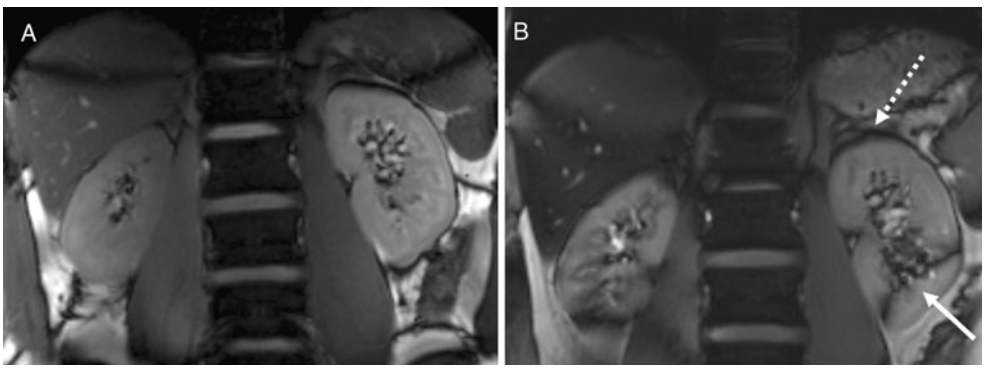

Fig. 6 TrueFISP images: **a** shows good depiction of the kidneys without relevant impairment by artefacts. In **b** banding artefacts associated with B_0 heterogeneities (*arrow*) could not be successfully shifted out of the region of interest. Minor chemical shift artefacts at the cranial margin of the left kidney were also noted (*dashed arrow*).

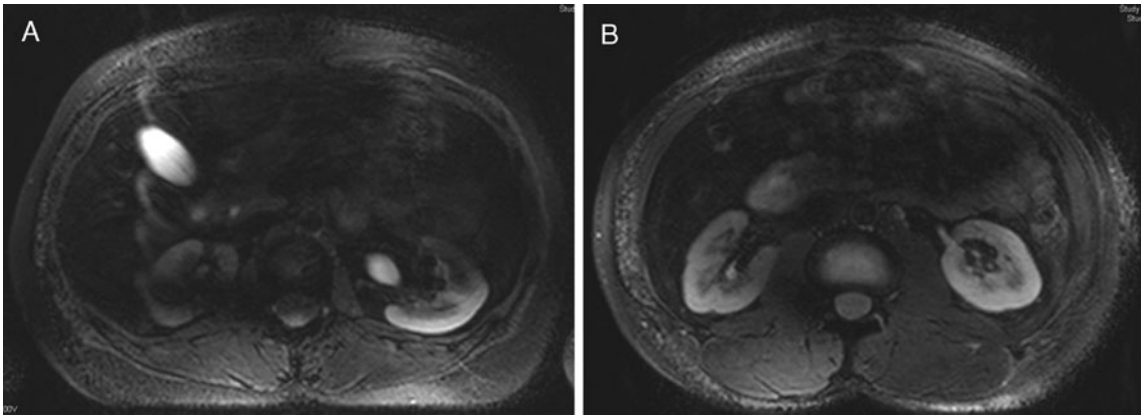

Fig. 7 T2-weighted TSE imaging remained strongly impaired, as imaging in 3 subjects did not deliver any diagnostic value (**a**). In the remaining 5 subjects (**b**), TSE imaging provided mediocre image quality with a mean quality score of 1.38

There are other options to overcome these restrictions in the future. The use of more powerful RF amplifiers and adiabatic pulses as well as the development of new coil concepts with more coil elements should surmount the current obstacles and enable improved signal homogeneity.

Another problem is affiliated with SAR restrictions at high-field MRI. SAR not only increases with the square of the magnetic field, but also with the square of the flip angle, the size of the patient, and also the duty cycle of the RF pulse, making SAR limitations especially problematic for the adequate acquisition of fast spin-echo and fat-saturated sequences. To mitigate the associated SAR increase, parallel imaging can be applied to reduce the number of excitation pulses, or flip angles can be decreased. In our study, despite using parallel imaging and a T2-weighted TSE sequence with variable flip angles, imaging still remained strongly limited owing to SAR.

As is known from other high field studies [2–4], T1 and T2 times at high field systems differ from known values at 1.5Tesla imaging, therefore measurements of T1 and T2 values of solid abdominal organs at 7 Tesla would have been desirable. However, owing to the above named B_1 field heterogeneities and the lack of RF power, no sufficient measurements were obtainable in breath-hold imaging. After surmounting these obstacles, further evaluations should be addressed in future studies.

Overall, our results should be considered as a first step towards human in vivo dedicated 7T renal MRI. Only a small number of healthy volunteers were incorporated. Thus, the value of this technique needs to be confirmed in patients with renal disease. Furthermore, the effect of intravenous gadolinium administration has to be evaluated in future investigations in order to investigate the benefits of dynamic imaging and perfusion analysis at 7T.

In conclusion, this first attempt at dedicated 7T kidney imaging reveals the diagnostic potential, but also the challenges and restrictions of ultra-high-field abdominal MRI. The initial imaging results demonstrate the successful transformation of the increased SNR into a high spatiotemporal resolution, yielding highly defined non-enhanced anatomical images while maintaining data acquisition within the window of a breath-hold with parallel imaging. Further optimisation of RF technology and dedicated coil concepts can be expected to better surmount the physical effects linked to high magnetic field strength and enable the acquisition of even greater image quality with corresponding clinical diagnostic value.

Acknowledgements This work was supported by the German Federal Ministry of Education and Research (BMBF), Grant No. 01EZ0716, which is administered by the German Aerospace Center (DLR).

References

1. Kinkel K, Lu Y, Both M et al (2002) Detection of hepatic metastases from cancers of the gastrointestinal tract by using noninvasive imaging methods (US, CT, MR imaging, PET): a meta-analysis 1. Radiology 224:748–756
2. Akisik FM, Sandrasegaran K, Aisen AM et al (2007) Abdominal MR imaging at 3.0 T. Radiographics 27:1433–1444
3. Barth MM, Smith MP, Pedrosa I et al (2007) Body MR imaging at 3.0 T: understanding the opportunities and challenges. Radiographics 27:1445–1462
4. Elmar MM, Brian MD, Erik KP (2006) Abdominal MR imaging at 3 T. Magn Reson Imaging Clin N Am 14:17–26
5. Lauenstein TC, Salman K, Saar B et al (2007) MR colonography: 1.5T versus 3T. Magn Reson Imaging Clin N Am 15:395–402
6. Ramalho M, Altun E, Heredia V et al (2007) Liver MR imaging: 1.5T versus 3T. Magn Reson Imaging Clin N Am 15:321
7. Ramalho M, Herédia V, Tsurusaki M et al (2009) Quantitative and qualitative comparison of 1.5 and 3.0 tesla MRI in patients with chronic liver diseases. J Magn Reson Imaging 29:869–879
8. Schindera ST, Merkle EM (2007) MR cholangiopancreatography: 1.5T versus 3T. Magn Reson Imaging Clin N Am 15:355–364
9. von Falkenhausen M, Meyer C, Lutterbey G et al (2007) Intra-individual comparison of image contrast in SPIO-enhanced liver MRI at 1.5T and 3.0T. Eur Radiol 17:1256–1261

10. Kollia K, Maderwald S, Putzki N et al (2009) First clinical study on ultra-high-field mr imaging in patients with multiple sclerosis: comparison of 1.5T and 7T. AJNR Am J Neuroradiol 30:699–702
11. Maderwald S, Ladd S, Gizewski E et al (2008) To TOF or not to TOF: strategies for non-contrast-enhanced intracranial MRA at 7 T. Magn Reson Mater Phys Biol Med 21:159–167
12. Mönninghoff C, Maderwald S, Theysohn JM et al (2009) Evaluation of intracranial aneurysms with 7 T versus 1.5 T time-of-flight MR Angiography"initial experience. Beurteilung von intrakraniellen Hirnarterienaneurysmen mit 7 Tesla versus 1, 5 Tesla-Time-of-Flight-MR-Angiografie"erste Erfahrungen. Rofo 181:16–23
13. Regatte RR, Schweitzer ME (2007) Ultra-high-field MRI of the musculoskeletal system at 7.0T. J Magn Reson Imaging 25:262–269
14. Bernstein MA, Huston J 3rd, Ward HA (2006) Imaging artifacts at 3.0T. J Magn Reson Imaging 24:735–746
15. Soher BJ, Dale BM, Merkle EM (2007) A review of MR physics: 3T versus 1.5T. Magn Reson Imaging Clin N Am 15:277–290
16. Banerjee S, Krug R, Carballido-Gamio J et al (2008) Rapid in vivo musculoskeletal MR with parallel imaging at 7T. Magn Reson Med 59:655–660
17. Behr B, Stadler J, Michaely H et al (2009) MR imaging of the human hand and wrist at 7 T. Skeletal Radiol 38:911–917
18. Vaughan JT, Snyder CJ, DelaBarre LJ et al (2009) Whole-body imaging at 7T: preliminary results. Magn Reson Med 61:244–248
19. Orzada S, Quick HH, Ladd ME et al (2009) A flexible 8-channel transmit/receive body coil for 7 T human imaging. Proceedings of the 17th Annual Meeting of ISMRM, Honolulu, HI, USA 2009 (Abstract 2999)
20. Bitz A, Brote I, Orzada S et al (2009) Am 8-channel add-on RF shimming system for whole-body 7 Tesla MRI including real-time SAR monitoring. Proceedings of the 17th Annual Meeting of ISMRM, HI, USA 2009 (Abstract 4767)
21. Christ A, Kainz W, Hahn EG et al (2010) The Virtual Family – development of surface-based anatomical models of two adults and two children for dosimetric simulations. Phys Med Biol 55:23–38
22. Snyder CJ, DelaBarre L, Metzger GJ et al (2009) Initial results of cardiac imaging at 7 Tesla. Magn Reson Med 61:517–524
23. Maderwald S, Orzada S, Schäfer LC et al (2009) 7T Human in vivo Cardiac Imaging with an 8-Channel Transmit/Receive Array. Proceedings of the 17th Annual Meeting of ISMRM, Honolulu USA 2009
24. Vikram R, Sandler CM, Ng CS (2009) Imaging and staging of transitional cell carcinoma: part 2, upper urinary tract. AJR Am J Roentgenol 192:1488–1493
25. Lauenstein TC, Salman K, Morreira R et al (2007) Nephrogenic systemic fibrosis: center case review. J Magn Reson Imaging 26:1198–1203